the plant journal

SEB SOCIETY FOR EXPERIMENTAL BIOLOGY

The Plant Journal (2025) **121,** e70028 doi: 10.1111/tpj.70028

The complex I subunit B22 contains a LYR domain that is crucial for an interaction with the mitochondrial acyl carrier protein SDAP1

Saurabh Saha[1], Simge Parlar[2], Etienne H. Meyer[2] and Monika W. Murcha[1,*]

[1]*School of Molecular Sciences and ARC Centre of Excellence in Plant Energy Biology, The University of Western Australia, Perth, Western Australia 6009, Australia, and*

[2]*Department of Cell Physiology, Institute of Biology, Martin-Luther-University Halle-Wittenberg, Weinbergweg 10, Halle (Saale) 06120, Germany*

Received 2 October 2024; revised 10 January 2025; accepted 24 January 2025.
*For correspondence (e-mail monika.murcha@uwa.edu.au).

SUMMARY

Mitochondrial complex I (CI), a large multi-subunit respiratory complex contains two LYR (leucine/tyrosine/arginine) domain-containing subunits, B14 (NDUA6/LYRM6) and B22 (NDUB9/LYRM3). Mitochondrial LYR (LYRM) proteins are soluble matrix-located proteins that have been implicated in diverse functions such as iron–sulphur cluster insertion, OXPHOS complex assembly, and mitoribosome biogenesis. B14 and B22 are unique to other LYRM proteins in that they are integral components of CI. To explore the function of B22, we examined T-DNA insertional knockout and knockdown lines, which displayed a mild growth defect linked to reduced CI activity and abundance. Notably, this defect could not be rescued by complementation with a B22 variant that contained a mutated LYR domain, indicating the domain's critical role in B22's function. Protein interaction assays further revealed that the LYR domain is crucial for B22's interaction with the neighbouring CI subunit, mitochondrial acyl carrier protein SDAP1. Similarly, T-DNA insertional knockdown lines of SDAP1 showed a comparable CI defect, suggesting that the interaction between B22 and SDAP1, mediated by the LYR domain, is important for the function and assembly of CI.

Keywords: LYR domain, B22 (NDUB9/LYRM3), assembly factors, NADH dehydrogenase, acyl carrier protein, OXPHOS biogenesis, SDAP (ACP), mitochondria, Arabidopsis, complex I.

INTRODUCTION

Mitochondria generate cellular energy through a linked series of chemical reactions known as oxidative phosphorylation (OXPHOS). It involves five multi-subunit enzyme complexes (CI-V) that are of bacterial origin (Lodish, 2016). The assembly of these complexes requires the highly regulated and co-ordinated transcription and translation of both nuclear and mitochondrial encoded subunits, the import and assembly of individual subunits, and protein maturation via the insertion of essential cofactors, such as iron–sulphur clusters (ISCs) (Ghifari et al., 2023; Meyer et al., 2019).

CI, also known as NADH dehydrogenase, is the first entry site of electrons in the OXPHOS reactions. It is the largest enzyme complex in the mitochondrial electron transport chain (ETC), and it catalyses the transfer of electrons from NADH to ubiquinone. The flow of electrons, results in an electromotive force that pumps protons across the inner mitochondrial membrane, which is later used for ATP production (Lodish, 2016). CI adopts an L-shaped architecture, with distinct modules dedicated to NADH oxidation (N), ubiquinone reduction (Q), and proton translocation (P_P – proton proximal and P_D – proton distal) all residing within its two arms – the membrane and the peripheral arm (Hofhaus et al., 1991; Wirth et al., 2016). In bacteria, CI consists of 14 subunits (Berrisford et al., 2016), whilst in plants, CI has expanded substantially in subunit composition. It also features a gamma carbonic anhydrase domain (CA) that is unique to plants (Klusch et al., 2021; Soufari et al., 2020). Recent structural determination in *Arabidopsis thaliana* (Arabidopsis) has revealed that plant CI consists of at least 48 subunits (Klusch et al., 2023).

In plants, four CI assembly factors have been identified to date. GLDH (L-galactono-1,4-lactone dehydrogenase), an enzyme that catalyses the last step of the ascorbate biosynthetic pathway was shown to be important for the assembly of the membrane arm (Leferink et al., 2008; Schertl et al., 2012; Schimmeyer et al., 2016).

INDH (iron–sulphur protein required for NADH dehydrogenase), an enzyme also referred to as Ind1 or NUBPL in humans was shown to be involved in ISC insertions (Bych et al., 2008; Sheftel et al., 2009; Wydro et al., 2013). NDUFAF1 (NADH:ubiquinone oxidoreductase complex assembly factor 1) was recently characterised in maize to be involved in the assembly of the membrane arm of CI (Wang et al., 2022). CIAF1 (CI assembly factor 1), a plant-specific LYR (leucine/tyrosine/arginine) domain-containing protein, was demonstrated to be involved in ISC insertion through its interaction with the 23 kDa subunit of CI (Ivanova et al., 2019). Interestingly, CI contains two bona fide LYR domain containing subunits, B14 (NDUA6) and B22 (NDUB9), the functions of which are still unknown (Angerer, 2015; Soufari et al., 2020). LYR proteins were originally assumed to have a role in ISC biogenesis, as the LYR motif containing protein ISD11 (Iron–Sulphur Domain 11) was shown to form a stable complex with cysteine desulfurase Nfs1, a central component of the mitochondrial ISC machinery, in yeast (Adam et al., 2006). However, other LYRM proteins have since then been shown to interact with the OXPHOS complexes either as assembly factors and/or through the recruitment of iron–sulphur clusters (ISCs) necessary for electron transport (Atkinson et al., 2011; Ivanova et al., 2019; Lefebvre-Legendre et al., 2001; Li et al., 2022).

Whilst most LYRM proteins identified to date are found as soluble proteins in the mitochondrial matrix, B14 and B22 are unique as they are the only LYRM proteins identified as subunits within the OXPHOS complexes. Additionally, two mitochondrial acyl carrier proteins (ACPs; also called SDAP) – SDAP1 and SDAP2, are found within close proximity to B22 and B14, respectively (Klusch et al., 2023; Soufari et al., 2020). ACPs are small soluble proteins involved in fatty acid biogenesis during which they act as a carrier of the synthesised fatty acid (Kastaniotis et al., 2017). Arabidopsis encodes for a third ACP, SDAP3; SDAP3 is annotated to be weakly expressed (Fu et al., 2020; Klepikova et al., 2016), whilst confirmed to be mitochondrial (Fuchs et al., 2020; Niehaus et al., 2020; Nietzel et al., 2020), it has not been identified as part of CI or any other complexes to date (Klusch et al., 2023). Also, it should be noted that SDAP3 is more divergent from SDAP1 and SDAP2 when comparing amino acid sequences. Its function is likely important for fatty acid biogenesis and lipoic acid biosynthesis as the double mutant *sdap1 sdap2* is viable but the triple mutant *sdap1 sdap2 sdap3* is not (Fu et al., 2020). Altogether, this suggests that the function of SDAP3 is limited to fatty acid biogenesis.

Their importance for fatty acid biogenesis is highlighted by the fact that the triple mutant is not viable (Fu et al., 2020). In yeast, it was shown that deletion of *B14* in *Yarrowia lipolytica* resulted in a loss of SDAP2, ultimately halting ubiquinone reductase activity (Angerer et al., 2014). Furthermore, a three-subunit protein bridge comprising of B14, SDAP2, and mFDX (mitochondrial ferredoxin-like protein) was observed in recently determined Cryo-EM structures of Arabidopsis and *Polytomella* sp. (Klusch et al., 2021, 2023). This bridge connects the ubiquinone module of the peripheral with the carbonic anhydrase domain and is thought to be important for CI function.

There are eight ISCs contained within five subunits of CI that form a chain through which electrons flow from the N module to the Q module in the matrix arm. Interestingly, B22 is positioned away from these clusters, at the tip of the membrane arm, suggesting that this LYR protein may have evolved to serve a different function within CI (Klusch et al., 2021; Soufari et al., 2020). In bovine, B22 is involved in a contact point between CI and CIII in the CI + CIII supercomplex through its interaction with UQCRC1 (ubiquinol-cytochrome *c* reductase) which is homologous to MPP-beta (mitochondrial-processing peptidase subunit beta) of plants (Letts et al., 2019). A similar interaction is observed in the Arabidopsis supercomplex I + III (Klusch et al., 2023). In Arabidopsis, it has been previously shown that deletion of B22 results in shorter roots, smaller size, and delayed flowering (Han et al., 2010), though the biochemical consequences of deleting B22 were not investigated.

Here we further investigated the function of the LYRM CI subunit, B22 in Arabidopsis. Phenotypic analysis revealed mild growth defects similar to those previously observed (Han et al., 2010), and these defects are restored when *b22* T-DNA insertional knockdown lines are complemented with B22. Biochemical analysis of mitochondria isolated from *b22* mutants reveals a CI defect that is restored when complemented with B22. Additionally, through protein interaction studies and structural predictions, we demonstrate that the LYR domain is essential for the interaction of B22 and the mitochondrial acyl carrier protein SDAP1. Interestingly, investigation of T-DNA insertion lines of SDAP1 reveals a similar CI defect that was observed for B22, confirming that B22 and SDAP1 are proteins both required for CI activity and their interaction is mediated by the LYR domain.

RESULTS

B22 is a mitochondrial CI subunit that contains a conserved LYR domain

B22 (At4g37400) is a small nuclear-encoded protein that consists of 117 amino acids and contains a conserved LYR (leucine/tyrosine/arginine) domain at position 23 and a conserved F (phenylalanine) at position 52 (Figure 1a,b). B22 has previously been identified as a mitochondrial CI subunit by proteomic analysis (Sunderhaus et al., 2006), and its structure within CI determined by Cryo-EM in

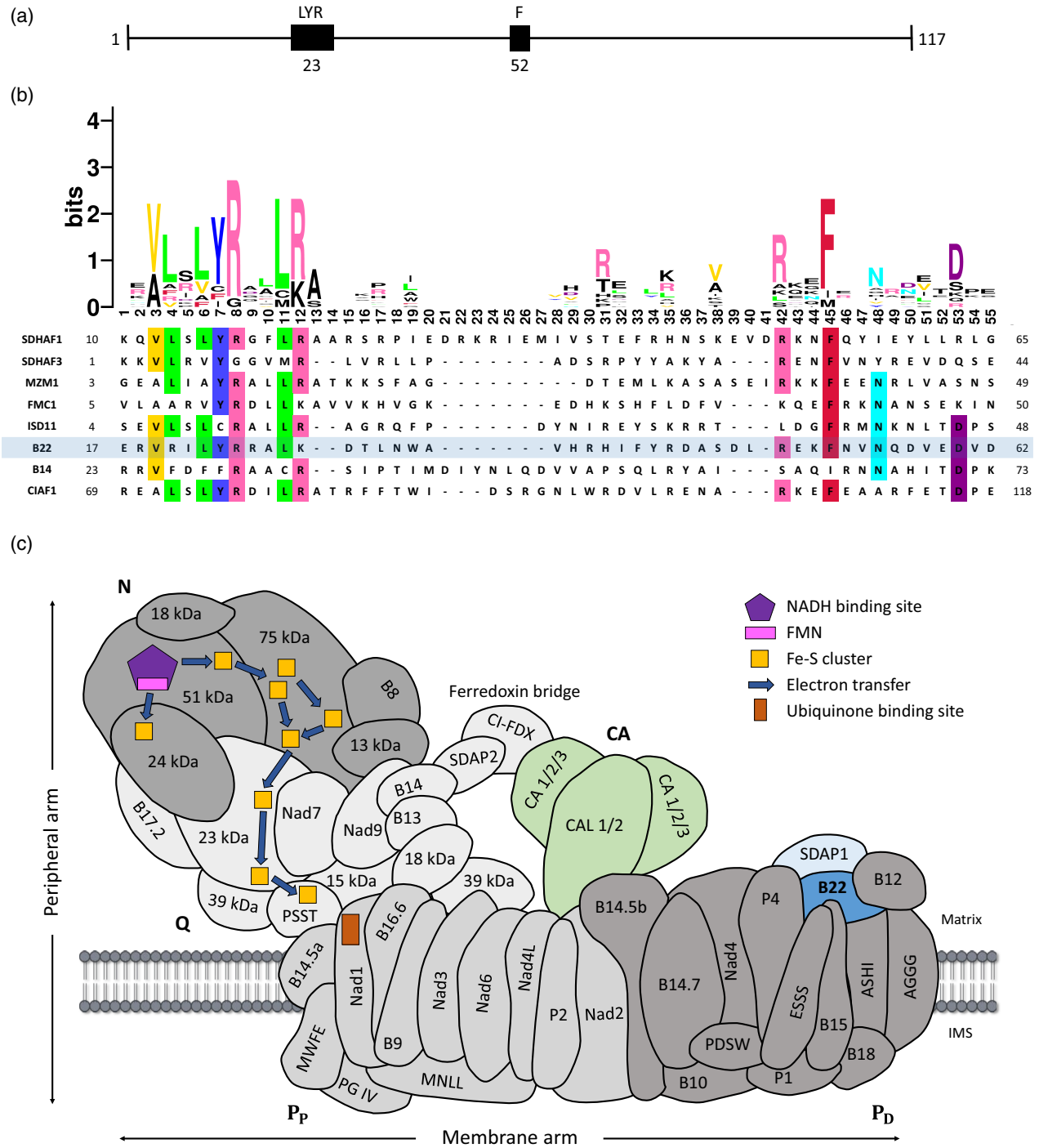

Figure 1. B22, a bonafide CI subunit, contains a highly conserved LYR domain.
(a) Protein model of B22 highlighting the LYR tripeptide sequence and the downstream F.
(b) A LOGO plot of B22 (highlighted in blue) with known LYR motif-containing proteins in Arabidopsis highlights the conserved tripeptide LYR (Leu/Tyr/Arg) and downstream F (Phe) motif.
(c) 2-D representation of CI subunits fitted to the Arabidopsis CI structure (PDB:7ARB) (Klusch et al., 2021). The various shades of grey highlight the modular design of CI: P_P, P_D – Proton translocation; Q – Quinone reduction; N – NADH oxidation; CA – Carbonic anhydrase (light green). B22 and SDAP1 are highlighted in blue and light blue, respectively.

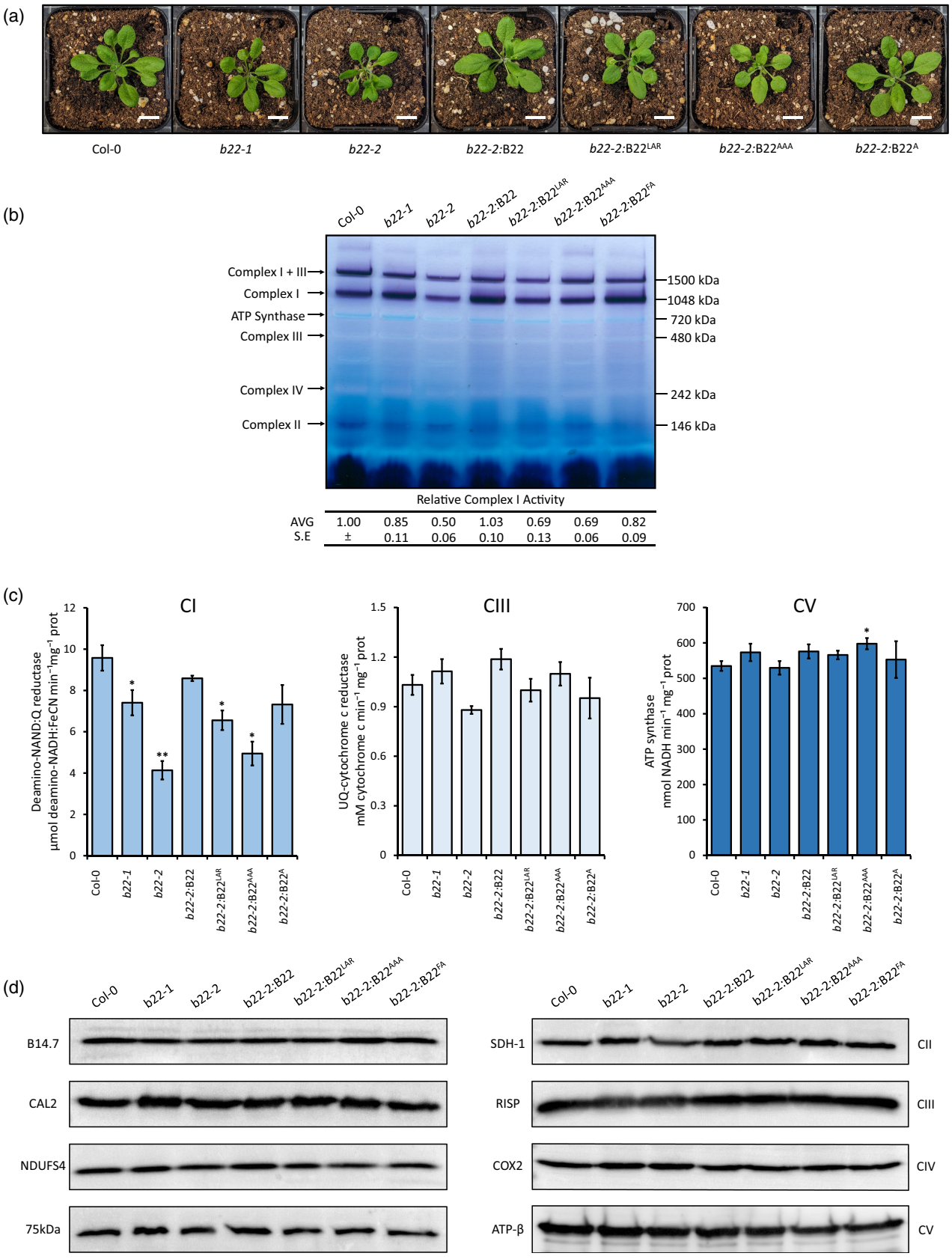

Figure 2. Reduced CI activity resulting from defective B22.
(a) Representative photographs of Col-0, *b22-1*, *b22-2*, *b22-2*:B22, *b22-2*:B22^{LAR}, *b22-2*:B22^{AAA}, and *b22-2*:B22^{A} on day 22. Scale bar = 1 cm.
(b) CI activity staining of isolated mitochondria from Col-0, *b22-1*, *b22-2*, *b22-2*:B22, *b22-2*:B22^{LAR}, *b22-2*:B22^{AAA}, and *b22-2*:B22^{A}, resolved on Blue Native PolyAcrylamide-Gel Electrophoresis. Quantification of CI and CI + III abundance relative to Col-0 was carried out using ImageJ ($n = 3$).
(c) Enzymatic activities of various mitochondrial respiratory complexes measured using isolated mitochondria from Col-0, *b22-1*, *b22-2*, *b22-2*:B22, *b22-2*:B22^{LAR}, *b22-2*:B22^{AAA}, and *b22-2*:B22^{A}.
(d) Immunodetection of antibodies raised against individual subunits of CI: NDUFS4, Cal2, B14.7, 75 kDa (left). Immunodetection of antibodies raised against other OXPHOS complexes: CII – SDH-1; CIII – RISP; CIV – COX2; CV – ATP-β synthase (right). Data represents mean ± SE ($\sigma/\sqrt{?}$); $^{*}P < 0.05$; $^{**}P < 0.001$ (determined by Student's *t*-test, $n = 4$).

Brassica oleracea (Soufari et al., 2020) and Arabidopsis (Klusch et al., 2021, 2023). B22 is located in the P_D module within close proximity to an acyl carrier protein (SDAP-1, mtACP1), distant from the chain of eight ISCs in the matrix arm domain (Figure 1c). Interestingly, this location suggests that B22 may not be directly involved in ISC biogenesis, unlike other LYR domain-containing proteins that have been characterised to date (Atkinson et al., 2011; Ivanova et al., 2019; Li et al., 2022).

Characterisation of *b22* knockdown and knockout lines

T-DNA insertional mutants for B22 (At4g34700); *b22-1* (SAIL_1146) and *b22-2* (SAIL_1240) were obtained, genotyped, and confirmed as knockdown lines by qRT-PCR, with *b22-1* and *b22-2* exhibiting respectively 36% and 9% in *B22* residual abundance (Figure S1b). Previous studies have shown the LYR domain has a role in recruiting the ISC complex (Li et al., 2022; Maio et al., 2014). To investigate the function of B22 and the LYR domain, complementation lines were generated using *b22-2* transformed with B22 and variants; B22^{LAR}, where tyrosine at position 21 was changed to alanine; B22^{AAA}, where the entire tripeptide LYR sequence was changed to AAA; and B22^{A}, where the conserved downstream phenylalanine (F) at position 52 was changed to alanine (Figure S1c). QRT-PCR was carried out on the complementation lines confirming the abundance of *B22* and its variants by at least 13-fold in the complementation lines (Figure S1d).

Analysis of mutant and complementation lines suggests that *b22-1* and *b22-2* exhibit mild growth defects (as previously observed; Han et al., 2010) that was restored by complementation with B22 (Figure 2a) and to a lesser extent B22^{A} (Figure 2a). Complementation with B22^{LAR} and B22^{AAA} did not restore the small growth delay observed in *b22-1* and *b22-2* (Figure 2a). To characterise this more comprehensively an early seedling growth stage progression analysis was carried out Arabidopsis seeds grown on ½ MS media with 3% (w/v) sucrose according to (Boyes et al., 2001). It was observed that *b22-1*, *b22-2*, and *b22-2*:B22^{A} took a significantly longer period of time to reach stage 1.02 compared with Col-0 (Figure S2a). Similar differences were found for *b22-2*:B22^{AAA} taking longer to reach stage 1.0, and for *b22-2*:B22^{LAR} and *b22-2*:B22^{A} to reach stage 1.04 (Figure S2a). These delays in growth were restored in the *b22-2*:B22 line (Figure S2a). Rosette size was also analysed on soil, with a significantly smaller rosette size observed for *b22-1* and *b22-2* on days 26, 29, and 32 compared with Col-0 (Figure S2b). This growth defect was restored in *b22-2*:B22 but not in *b22-2*:B22^{LAR}, *b22-2*:B22^{AAA}, or *b22-2*:B22^{A} (Figure S2b). Notably, Col-0 leaves were up to 6 cm longer than those of the *b22-2* mutant on day 32 (Figure S2b, Student's *t*-test, $^{*}P < 0.05$, $^{**}P < 0.001$, $n = 18$).

To investigate the consequences of mitochondrial function during plant development, root and hypocotyl length were measured for all lines. It was observed that the *b22-2* and *b22-2*:B22^{AAA} mutants exhibited significantly shorter root lengths on 3% (w/v) sucrose medium compared to Col-0 after 10 days of growth and when grown on 0% (w/v) sucrose media, significantly shorter root length was observed in *b22-1* (Figure S2c, Student's *t*-test, $^{*}P < 0.05$, $^{**}P < 0.001$, $n = 20$). Significantly shorter hypocotyl lengths were observed in *b22-1*, *b22-2*, *b22-2*:B22^{LAR}, *b22-2*:B22^{AAA}, and *b22-2*:B22^{A} compared with Col-0 at 10 days (Figure S2d, Student's *t*-test, $^{*}P < 0.05$, $^{**}P < 0.001$, $n > 27$).

Additionally, a third T-DNA mutant, *b22-3* (SAIL_251), was also studied and confirmed as a knockout by qRT-PCR, showing no detectable transcript levels (Figure S7a). This mutant exhibited a more pronounced growth phenotype 11 days after imbibition (Figure S7b).

B22 mutants exhibit lower CI activity and abundance

To investigate whether the observed phenotypes resulted from defective CI, mitochondria were isolated from 14-day-old seedlings of all lines and resolved by Blue Native PolyAcrylamide-Gel Electrophoresis (BN-PAGE) followed by in-gel NADH dehydrogenase activity staining as previously described (Schertl & Braun, 2015) (Figure 2b). The BN-PAGE analysis and subsequent CI staining revealed a significant decrease in CI activity/abundance of up to 50% for *b22-2* and a mild decrease of up to 15% for *b22-1*, whilst the complementation line *b22-2*:B22 and the mutant *b22-2*:B22^{A} restored of CI activity/abundance to similar levels as observed in Col-0 (Figure 2b). Interestingly, a significant decrease of 25–30% was also seen for the mutants, *b22-2*:B22^{LAR} and *b22-2*:B22^{AAA} (Figure 2b).

To confirm these observations, spectrometric enzymatic activity assays for CI, CIII, and CV were carried out on isolated mitochondria from Col-0 and all mutants. A significant reduction in CI activity was observed in both the

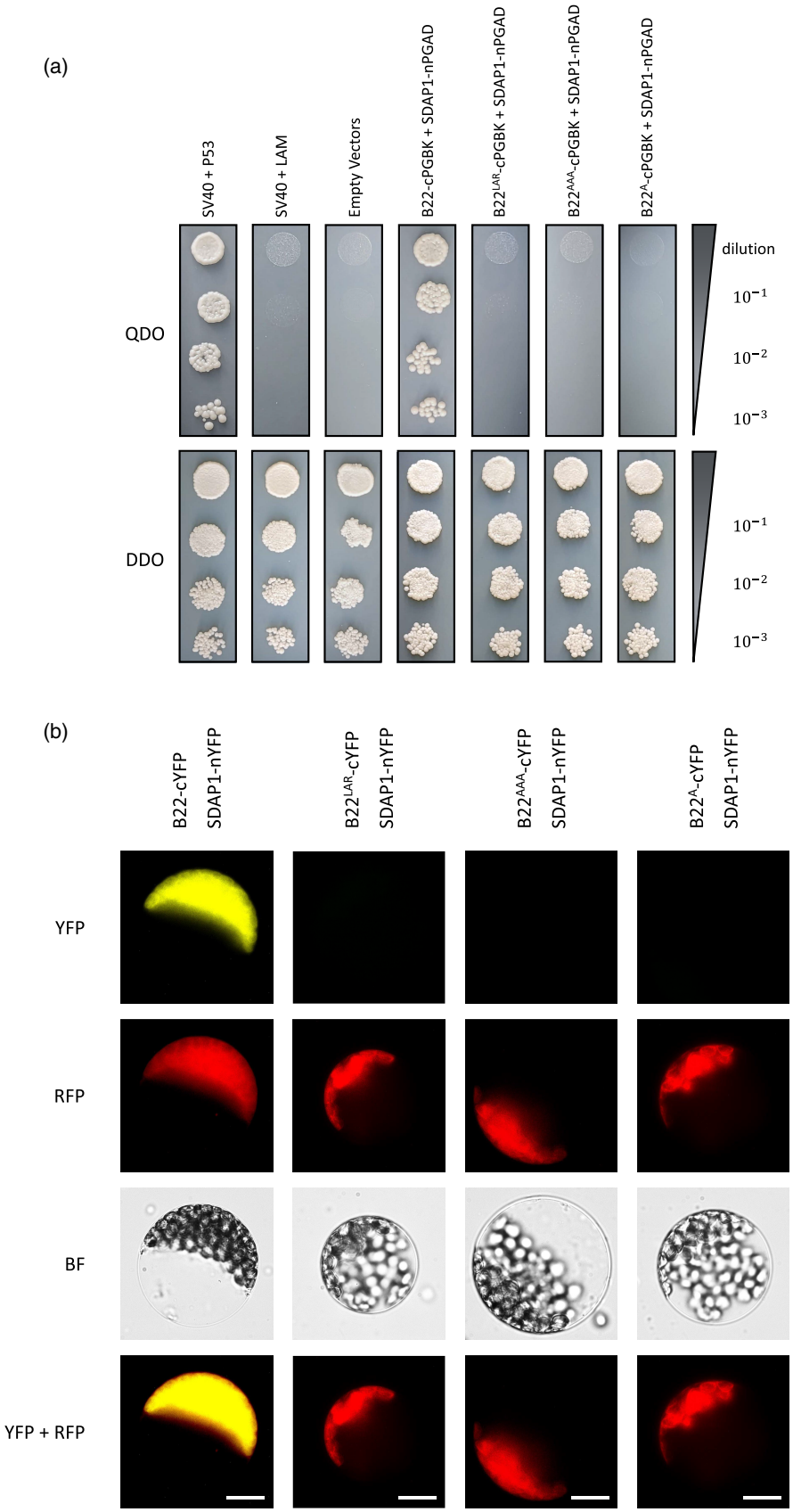

Figure 3. B22 interacts with the mitochondrial acyl carrier protein, SDAP1.
(a) Yeast-2-Hybrid interaction assay of SDAP1 and B22, both with and without a defective LYR domain. Successful mating was determined by growth on DDO, whilst positive interactions were identified by growth on QDO. SV40 antigen and p53/LAM interactions served as positive and negative controls, respectively. No interactions were observed using empty vectors.
(b) Bimolecular fluorescence complementation assays of B22, $B22^{LAR}$, $B22^{AAA}$, and $B22^{A}$, with SDAP1 in Arabidopsis mesophyll protoplasts transfected with constructs encoding either the C-terminal or N-terminal half of yellow fluorescent protein (cYFP/nYFP). Scale bar = 20 μm.

mutant lines, *b22-1* and *b22-2*, by 23% and 57%, respectively, and *b22-2*:$B22^{LAR}$ and *b22-2*:$B22^{AAA}$, by 32% and 49%, respectively (Figure 2c). This reduction was more apparent in the lines, *b22-2* and *b22-2*:$B22^{AAA}$, exhibiting approximately half the activity when compared to Col-0. Furthermore, the activity of the complemented line, *b22-2*:B22, and the mutant, *b22-2*:$B22^{A}$ was restored to that of Col-0. Activity levels for CIII and CV showed no significant changes for all the mutants (determined by Student's *t*-test, $n = 4$).

Protein abundance of various individual CI subunits was investigated through immunodetection of isolated mitochondria. Immunodetection of subunits B14.7, CAL2, NDUFS4, and the matrix domain 75 kDa subunit show no obvious changes to subunit abundance (Figure 2d). Furthermore, immunodetection of CII subunit, SDH-1, CIII subunit RISP, CIV subunit Cox2, and ATP synthase subunit ATP-β revealed no obvious difference in their abundance (Figure 2d).

B22 interacts with the acyl carrier protein SDAP1 via the LYR domain

Recently, the Cryo-EM structure of the human ISC complex revealed that ISD11/LYRM4 is in close proximity to SDAP, a mitochondrial acyl carrier protein (Fox et al., 2019). The interaction between LYRM proteins and ACP has also been documented in other eukaryotes (Boniecki et al., 2017; Maio et al., 2014; Vranken et al., 2018), mediated by the LYR domain, it is proposed that acetylated ACP acts as an allosteric activator of LYRM proteins. In the recently determined CI Cryo-EM structures from Arabidopsis and *Brassica oleracea*, the two LYR proteins, B14 and B22 were also found to be in close proximity to SDAP2 and SDAP1 respectively (Klusch et al., 2023; Soufari et al., 2020) (Figure 1c).

Therefore, to confirm that Arabidopsis B22 interacts with SDAP1, and to determine if the LYR domain is essential for this interaction, we conducted protein interaction assays using Y2H assays and BiFC. Mating competent yeast was transformed with expression vector for either B22, $B22^{LAR}$, $B22^{AAA}$, or $B22^{A}$ and mated with compatible yeast cells transformed with vectors for the expression of various CI subunits including B8, Cal2, Ca3, 75 kDa, 23 kDa, PSST, B13, 13 kDa, P1, MNLL (Ivanova et al., 2019), SDAP1, and SDAP2, as well as ISC biogenesis proteins ISU1, HSCB, HSP23.5, and HSP23.6 (Li et al., 2022). Positive protein–protein interactions were observed with B22-cpPGBK and SDAP1-npgbk only (Figure 3a). Mutation of the LYR and F domains $B22^{LAR}$, $B22^{AAA}$, and $B22^{A}$ abolished any interaction with B22 (Figure 3a).

To confirm these interactions *in planta*, BiFC analysis was performed using Arabidopsis protoplasts. Co-transformation of B22-cYFP and SDAP1-nYFP resulted in a reconstituted YFP fluorescence (Figure 3b), whereas co-transformation of SDAP1-nYFP with any of the LYR variants ($B22^{LAR}$-nYFP, $B22^{AAA}$-nYFP, and $B22^{A}$-nYFP) did not yield reconstituted YFP fluorescence (Figure 3b). These findings confirm that B22 interacts with SDAP1 and the conserved LYR domain and the F residue are required for this interaction. Known interacting mitochondrial proteins Tim17 and Tim23 were used as positive controls (Figure S3).

To gain insights into the structural basis of the observed interactions, structural predictions were carried out using AlphaFold-3 (Jumper et al., 2021) to predict the putative structures of the interacting pairs SDAP1:B22, SDAP1:$B22^{LAR}$, SDAP1:$B22^{AAA}$, and SDAP1:$B22^{A}$. Predicted aligned errors of these models and interaction sites are given in Figure S6.

The closest contact points (pseudo-bonds >3 Å) of the putative tertiary structure of SDAP1:B22 in the AlphaFold-3 model were predicted to be located within the L_{23} and R_{49} regions of the B22 protein (Figure 4a). Specifically, the tyrosine residue (Y_{24}) was predicted to form a hydrogen bond with glutamate (E_{88}) in SDAP1, whilst arginine (R_{25}) was predicted to form at least four hydrogen bonds with glutamate (E_{94}) and aspartic acid (D_{103}) in SDAP1 (Figure 4b). Upon mutation of tyrosine (Y_{24}) to alanine (A_{24}), AlphaFold predicts that there is no longer an interaction with glutamate (E_{88}). Furthermore, it also affects the ability of the arginine (R_{25}) to interact with glutamate (E_{94}) by losing up to three hydrogen bonds (Figure 4b). Lastly, when mutating the LYR tripeptide sequence to AAA, all interactions with the SDAP1 molecule are lost, suggesting that this region is essential for an interaction between B22 and SDAP1 (Figure 4b).

Additionally, in the predicted SDAP1:B22 structure, the arginine (R_{49}), an amino acid that is also conserved amongst some LYR proteins (Figure 1b), was predicted to form three hydrogen bonds with aspartic acid (D_{85}) and glutamate (E_{88}). Interestingly, upon mutating the conserved phenylalanine (F_{52}) to alanine, two of these hydrogen bonds are lost, indicating that this region must also be necessary for the interaction between B22 and SDAP1

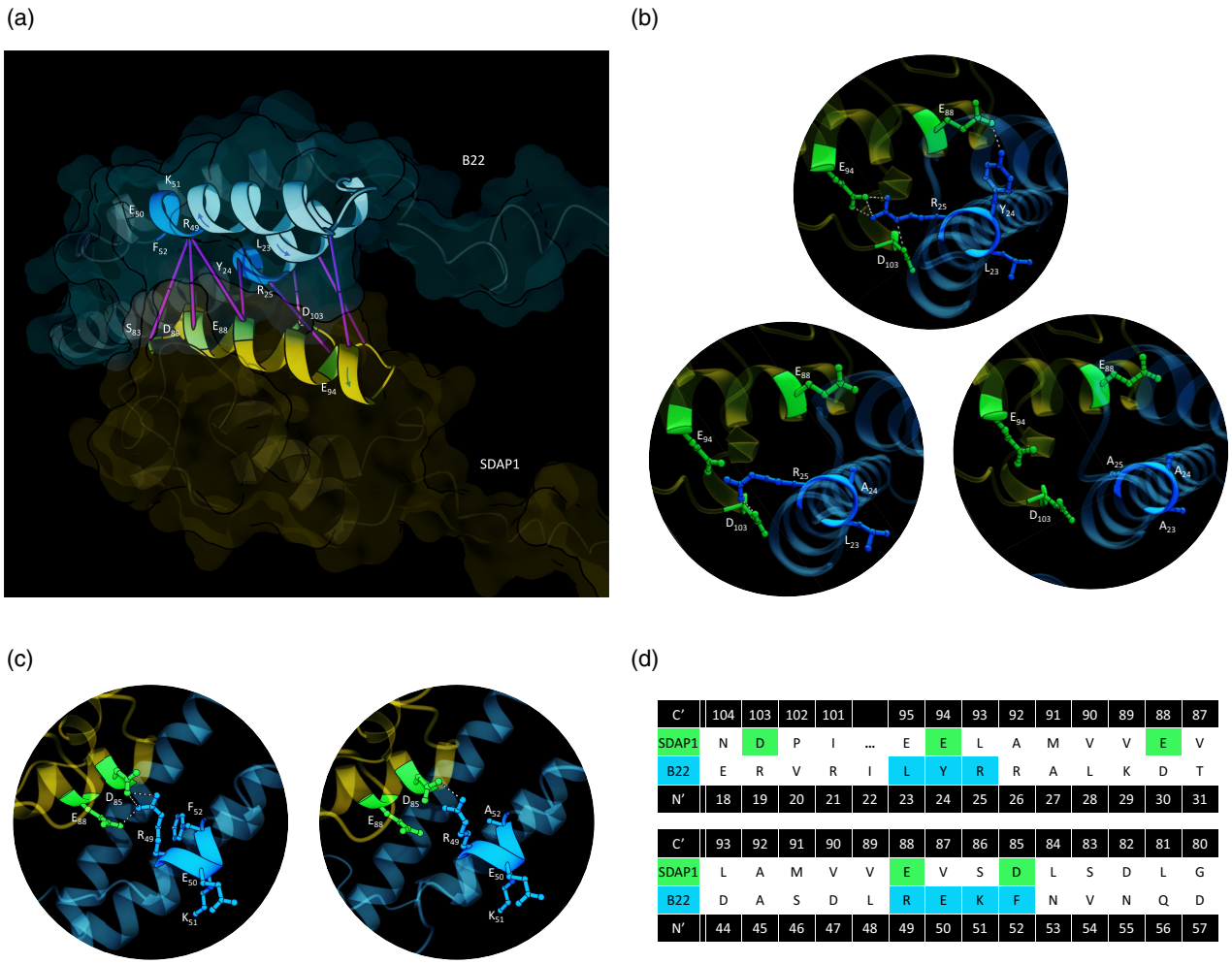

C′	104	103	102	101		95	94	93	92	91	90	89	88	87
SDAP1	N	D	P	I	…	E	E	L	A	M	V	V	E	V
B22	E	R	V	R	I	L	Y	R	R	A	L	K	D	T
N′	18	19	20	21	22	23	24	25	26	27	28	29	30	31

C′	93	92	91	90	89	88	87	86	85	84	83	82	81	80
SDAP1	L	A	M	V	V	E	V	S	D	L	S	D	L	G
B22	D	A	S	D	L	R	E	K	F	N	V	N	Q	D
N′	44	45	46	47	48	49	50	51	52	53	54	55	56	57

Figure 4. Predicted tertiary protein structures of B22 and SDAP1 using AlphaFold v3 (Jumper et al., 2021).
(a) Tertiary protein structure of B22 and SDAP1 with highlighted predicted pseudo-bonds (>3 Å) in purple.
(b) Predicted structure of B22's interaction with SDAP1 through the LYR domain and the mutated LAR/AAA. Hydrogen bonds (H–N) are represented using dotted lines.
(c) Predicted structure of B22's interaction with SDAP1 in the downstream F region and the mutated F→A region.
(d) Sequence alignment of B22 and SDAP1, highlighting the regions that form hydrogen bonds.

(Figure 4c). Amino acid residues of the predicted interacting regions are highlighted in green (Figure 4d).

To ensure the reliability of our structural predictions, we also modelled these interactions using AF2-MM and ChAi-1 (Boitreaud et al., 2024; Evans et al., 2022). In both the AF2-MM and ChAi-1 models, the tyrosine residue (Y_{24}) was predicted to form a hydrogen bond with glutamate (E_{88}) in SDAP1, consistent with our AlphaFold-3 model (Figures S4a and S5a). Furthermore, arginine (R_{25}) was predicted to form a hydrogen bond with either aspartic acid (D_{103}) or glutamate (E_{94}), in the AF2-MM and ChAi-1 models, respectively (Figures S4a and S5a). Upon mutation of the LYR tripeptide sequence to either LAR or AAA, the AF2-MM model predicted no interaction with SDAP1 (Figure S4a). Additional residues of SDAP1 predicted to interact in these models are highlighted in yellow (Figure 4d).

Additionally, the conserved arginine (R_{49}) of B22 was predicted to form a hydrogen bond with aspartic acid (D_{82}) instead of (D_{85}), and this interaction remained intact despite mutating phenylalanine (F_{52}) to alanine in the AF2-MM model (Figure S4b). Interestingly, the ChAi-1 model predicted an N-terminal insertion of SDAP1 between the three alpha helices of B22. Upon mutation of either the LYR tripeptide or the downstream (F52), this insertion was no longer observed (Figure S5b).

Deletion of the acyl carrier protein SDAP1 results in defective CI abundance and assembly

We also carried out a genetic approach to confirm the link between SDAP1 and B22. For this, single and double mutants for the three SDAP homologues (*sdap1*, *sdap2*, *sdap3*, *sdap1−/−sdap2*, *sdap1−/−sdap3*, and

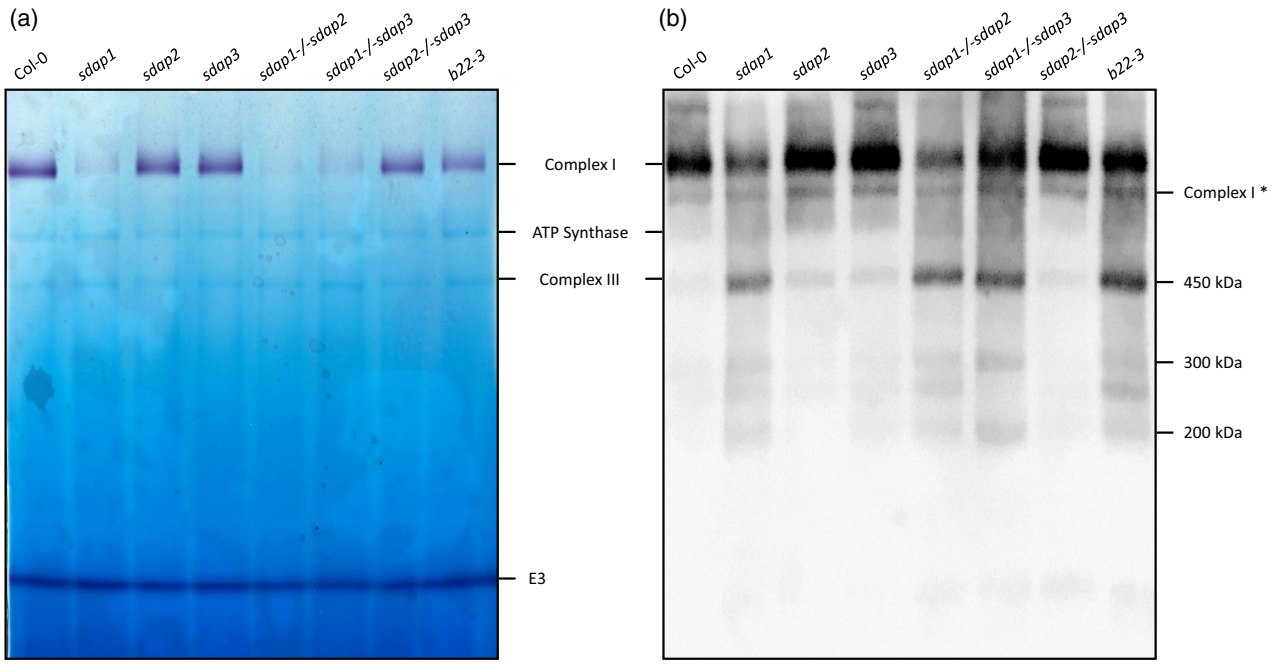

Figure 5. The absence of B22 or SDAP1 leads to similar assembly defects.
(a) NADH dehydrogenase activity staining of complexes separated by BN-PAGE. The staining of the E3 subunit of the PDC serves as loading control.
(b) Immunodetection of CI assembly intermediates using the anti-CA2 antibodies.

sdap2−/−sdap3) were obtained (Fu et al., 2020) and compared with the *b22-3* mutant. Mitochondria were isolated from each line and CI activity and abundance was investigated using BN-PAGE and in-gel activity assays. NADH dehydrogenase activity staining shows low levels of CI in mitochondria isolated from *sdap1* and *b22-3* whereas the lines *sdap2* and *sdap3* show similar levels of CI to Col-0 (Figure 5a). The mitochondrial samples used for this analysis were kept frozen for several weeks, which may have destabilised supercomplexes, contributing to the reduced visibility of the I + III supercomplex in the gel (Figure 5a). To investigate CI assembly in these lines, mitochondrial complexes were resolved on a BN-PAGE gel, transferred onto a nitrocellulose membrane, and immunodetected using anti-CA2. This allows for the detection of assembly intermediates of the membrane arm of CI. In *b22-3*, an assembly intermediate of 450 kDa was more pronounced, in addition to weaker bands representing the CA2-containing intermediates of ~200 and ~300 kDa (Figure 5b), suggesting a defect in the assembly of the full monomeric CI. A very similar pattern is observed in *sdap1* and both double mutants containing *sdap1*. Immunodetection with anti-CA2 identifies the last assembly intermediate of CI (CI*) and no variation was found in the abundance of CI* across the samples (Figure 5b). Altogether, this analysis confirms that SDAP1, but not SDAP2 or SDAP3, interacts with B22, and this interaction is important for efficient CI biogenesis.

DISCUSSION

CI plays a central role in mitochondrial respiration as the first site of electron transport during OXPHOS. CI is composed of 48 individual subunits, many of whose function has yet to be determined. This study investigates the role of B22, a nuclear-encoded CI subunit. B22 belongs to the LYRM protein family, a conserved family of eukaryotic proteins involved in regulating core mitochondrial functions such as ISC recruitment, translation, and OXPHOS complex assembly (Angerer, 2015; Dohnálek & Doležal, 2024). Our results demonstrate that B22 is important for the proper function of CI. Phenotypic analysis of T-DNA insertional lines for B22 revealed a mild but statistically significant growth defect with reduced hypocotyl and root lengths suggesting a developmental impact due to compromised CI function (Figure S2). The mild growth defect correlated with a decrease in CI abundance and activity as determined by BN-PAGE in-gel CI activity staining and activity assays using isolated mitochondria and as no significant defect was observed in CIII or CV activity, we propose that the growth defect can be attributed to a decrease in CI activity alone (Figure 2b,c). Interestingly, the abundance of individual CI subunits, such as B14.7, CAL2, NDUFS4, and the 75 kDA subunit remained unchanged when determined by immunodetection, implying that the decrease in CI abundance and activity is due to a defect in the assembly or stability of the monomeric CI complex and not the abundance

The Plant Journal published by Society for Experimental Biology and John Wiley & Sons Ltd.,
The Plant Journal, (2025), doi: 10.1111/tpj.70028

of individual CI subunits (Figure 2d). This has previously been observed with mutant lines of the CI assembly factor, CIAF1, another LYR domain-containing protein (Ivanova et al., 2019). CIAF1 unlike B22, is matrix-located, and was shown to assist in Fe-S cluster insertion within a matrix arm domain subunit. A knockdown of this protein resulted in a much more severe CI defect, with almost no monomeric CI being detected, instead an assembly intermediate was present consisting of the membrane arm domain modules (Ivanova et al., 2019). In this study, we tested the ability of B22 to interact with ISC subunits and various other Fe–S clusters containing CI subunits but did not observe any interaction. This suggests that the function of B22 may not be in ISC cluster recruitment as we previously determined for CIAF1, and for another LYRM protein Succinate Dehydrogenase Assembly Factor 1 (SDHAF1) which we determined to be involved in ISC cluster insertion within the SDH subunit SDH2 (Li et al., 2022).

Whilst mitochondrial ACPs are thought to exist predominantly as soluble matrix proteins involved in fatty acid synthesis (Fu et al., 2020), an increasing number of studies show that ACP associates with LYRM proteins. ACPs have been identified alongside LYRM proteins in CI in both plants and non-plants (Cronan et al., 2005; Klusch et al., 2023; Soufari et al., 2020), the ISC complex (Boniecki et al., 2017; Cory et al., 2017; Floyd et al., 2016; Fox et al., 2019; Herrera et al., 2018), and in mitoribosomes (Itoh et al., 2022; Vranken et al., 2018). The ability of LYRM proteins to interact with ACP has been hypothesised to be a mechanism for regulating mitochondrial metabolism, whereby an acetylated ACP, upon interaction with an LYRM protein, acts as a signalling molecule to trigger ISC insertion, assembly, or protein synthesis (Dohnálek & Doležal, 2024; Masud et al., 2019; Nowinski et al., 2018).

Evolutionary analysis shows that across the various eukaryotic lineages, LYRM subfamilies are conserved, and present alongside ACPs (Dohnálek & Doležal, 2024). Furthermore, structural predictions reveal that despite diverse functions and low sequence homology all LYRM proteins are able to form a three alpha-helical tunnel structure that can fit the acyl moiety of an acetylated ACP (Dohnálek & Doležal, 2024).

In plants, Cryo-EM analysis revealed that B22 is near an ACP, named SDAP1 (Klusch et al., 2023; Soufari et al., 2020). Here, we confirmed the ability of SDAP1 (but not SDAP2) to interact with B22 using both Y2H interaction assays and BiFC analysis in Arabidopsis protoplasts (Figure 3a,b). Furthermore, this interaction was abolished when the LYR domain was mutated, confirming the LYR/F residues are necessary for this interaction to occur. To further investigate the role of the conserved LYR domain within B22, we carried genetic complementation assays whereby the *b22-2* line was complemented with wild-type B22 or B22 containing mutated LYR residues ($B22^{LAR}$, $B22^{AAA}$, $B22^{A}$) (Figure 2b,c). The LAR and AAA variants failed to restore the CI abundance and activity back to wild-type levels. The *b22-1*:$B22^{A}$ mutant partially rescued CI activity. Although our Y2H and BiFC assays did not detect an interaction between $B22^{A}$ and SDAP1, it is possible that these proteins assemble in planta through a weaker interaction that these methods were unable to detect. Supporting this possibility, our AlphaFold-3 and AF2-MM models suggest that R_{49}, rather than F_{52}, makes contact with SDAP1, indicating that the F_{52} mutation might still permit a weaker interaction within the plant context (Figure 4c; Figure S4b). Our experiments confirm that the LYR domain (and possibly the conserved F) is important for the function of B22 in maintaining CI integrity and function and this is most likely via an interaction with SDAP1. Similar experiments have previously been carried out with the CI subunit B14, in yeast. The LYR domain within B14 was mutated and identified to be required for CI activity and stability in *Yarrowia lipolytica*. Interestingly, mutation of the LYR/F domain also abolished any association of ACP with CI (Angerer et al., 2014).

To further investigate the link between ACP and B22, we characterised T-DNA insertional knockdown lines for mitochondrial ACPs. Arabidopsis encodes for three SDAP (SDAP1, SDAP2 and SDAP3) (Meyer et al., 2007), analysis of mitochondria isolated from single and double mutant variants showed that only the knockdown lines containing *sdap1* exhibited a CI defect, in agreement with our interaction studies. We also observed a 450 kDa assembly intermediate in mitochondria isolated from *sdap1* and *b22* mutants suggesting that the assembly of the membrane arm domain submodule was compromised (Figure 5b). A similar defect has been observed in mutants of a mitochondrial acyl carrier protein from *Neurospora crassa* (acp-1), where deletion of acp-1 affects the assembly of the membrane arm of CI and also leads to a loss of peripheral arm subunits (Schneider et al., 1995). However, it is noteworthy that the SDAP1 mutation had a more pronounced impact on CI levels than the B22 mutation (Figure 5a). This suggests that whilst both proteins interact and contribute to CI biogenesis, SDAP1 may also interact with other CI LYR domain-containing proteins.

Here, we show that in Arabidopsis, the CI subunit B22 and the acyl carrier protein SDAP1, interact via the LYR domain, to maintain CI abundance and activity. We have identified a likely assembly intermediate generated upon deletion of these subunits, and it would be fascinating to determine if these subunits play a specific role in the assembly of CI or in maintaining the stability of an already assembled CI. Furthermore, the intriguing question remains as to how acyl modification of the ACP can regulate the biogenesis of CI via B22 which likely acts as an adapter protein. It would be exciting to propose that the acylation state of ACP is a regulatory mechanism for

controlling OXPHOS complexes, allowing for rapid control of OXPHOS function to respond to mitochondrial homeostasis and energy demands.

MATERIALS AND METHODS

Bioinformatic analysis

Protein sequences for Arabidopsis LYR proteins (SDHAF1, SDHAF3, MZM1, FMC1, ISD11, B22, B14, and CIAF1) were retrieved from The Arabidopsis Information Resource (TAIR). Sequence alignment was performed using ClustalW, and a logo map was generated using WebLogo with standard parameters (Berardini et al., 2015; Crooks et al., 2004; McWilliam et al., 2013).

Cloning and plasmid construction

The protein-encoding sequence of B22 (At4g34700) was amplified from Arabidopsis Col-0 complementary DNA (cDNA) using gene-specific primers (Table S1) flanked by Gateway recombination cassettes and cloned into pDONR207. Site-directed mutagenesis was conducted utilising a QuikChange kit (Stratagene) to generate three variants: $B22^{LAR}$, $B22^{AAA}$, and $B22^{A}$ with primers specified in (Table S1). These genes were recombined into various plasmids: pMDC43 for *Agrobacterium tumefaciens*-mediated transformation (Karimi et al., 2002); pGBKCg/pGBKT7 and pGADCg/pGADT7g for Yeast-2-Hybrid (Y2H) interaction assays (Stellberger et al., 2010); and pSAT4-DEST-nEYFP-C1 (pE3136), pSAT4-DEST-nEYFP-N1 (pE3134), pSAT5-DEST-cEYFP-C1 (pE3130), and pSAT5-DEST-cEYFP-N1 (pE3132) for bimolecular fluorescence complementation (BiFC) assays (Hua et al., 2018).

Plant materials and growth conditions

Col-0 and mutant seeds were surface sterilised with chlorine gas, germinated on half-strength MS salt medium (½ MS) containing 1.5% (w/v) sucrose, and grown under a 16-h photoperiod at 22 ± 2°C with a light intensity of 80 μmol quant m^{-2} sec^{-1} (standard growth conditions). For soil-based analysis, a mixture of peat moss, perlite, and vermiculite (3:1:1) was used under the same growth conditions. Arabidopsis *b22* T-DNA insertional lines (SAIL_1146_B01, SAIL_1240_D04, and SAIL_251_C09) were acquired from ABRC (Arabidopsis Biological Resource Centre) and NASC (Nottingham Arabidopsis Seed Centre) and confirmed as homozygous loss-of-function mutants through antibiotic selection and PCR using primers listed (Table S1). Loss of function was confirmed by quantitative real-time PCR (qRT-PCR) analysis. The lines were denoted as *b22-1* (SAIL_1146_B01), *b22-2* (SAIL_1240_D04), and *b22-3* (SAIL_251_C09). Complementation was carried out using *b22-2* and pMDC43–B22, pMDC43-$B22^{LAR}$, pMDC43-$B22^{AAA}$, and pMDC43-$B22^{A}$ constructs (Figure S1c) via *Agrobacterium tumefaciens*-mediated transformation as described in (Karimi et al., 2002). Complemented lines were denoted as *b22-2*:B22, b22-2:$B22^{LAR}$, *b22-2*:$B22^{AAA}$, and *b22-2*:$B22^{A}$.

Phenotypic analysis

Col-0 and mutant seeds were stratified for 3 days at 4°C in a dark room to ensure synchronised growth for all phenotypic analysis. Stage growth analysis and rosette leaf measurements were conducted according to parameters previously described by Boyes et al. (2001) (n = 18). For root length analysis, seeds were sown on ½ MS with either 0 and 1.5% (w/v) sucrose and positioned vertically under standard growth conditions for 10 days (n = 20). Hypocotyl elongation was carried out on ½ MS plates with 1.5% (w/v) sucrose and positioned vertically in the dark for 10 days (n > 27). Roots were photographed and lengths were determined using ImageJ (Schneider et al., 2012).

Quantitative real-time PCR

RNA was extracted from 14-day-old seedlings using the FavorPrep Total RNA Purification Mini Kit (Favorgen, Ping Tung, Taiwan) according to manufacturer's instructions. cDNA synthesis was carried out using a High-Capacity cDNA Reverse Transcription Kit (Applied Biosystem, Waltham, MA, USA). Standards for the reference gene *ACTIN2* (AT3g18780) and *B22* was amplified using primers listed in Table S1. QRT-PCR was carried out in a LightCycler 480 (Roche, Basel, Switzerland) using SYBR Green master mix (Roche, BIO-RAD, Hercules, CA, USA). All samples were normalised using *ACTIN2*, and measurements were technically replicated twice on RNA isolated from two independent seedling populations.

Mitochondrial isolation, gel electrophoresis, and immunoblotting

Mitochondria were isolated under cold conditions from 14-day-old seedlings grown in sterilised pots containing ½ MS liquid medium under standard growth conditions with agitation at 200 rpm as previously described (Murcha & Whelan, 2015).

Blue Native PolyAcrylamide-Gel Electrophoresis (BN-PAGE) was carried out using 30 μg of isolated mitochondria, solubilised in 5% (w/v) digitonin and resolved using precast NativePAGE 4–16% Bis-Tris gels (Invitrogen) (Eubel et al., 2005). CI in-gel activity staining was carried out as previously described (Schertl & Braun, 2015). Quantification of gel bands was carried out using ImageJ (Schneider et al., 2012) (n = 3).

Proteins were separated on 12% (w/v) SDS-PAGE denaturing gels and transferred to a polyvinylidene fluoride (PVDF) membrane. Immunodetection was carried out using antibodies raised against NDUFS4 (Meyer et al., 2009), 75 kDa (PhytoAb, USA), CA2 (Perales et al., 2005), CAL2 (Fromm et al., 2016), B14.7 (Wang et al., 2012), SDH-1 (Peters et al., 2012), RISP (Carrie et al., 2010), COX2 (AGRISERA), and ATP-β (AGRISERA).

Activity assays

All enzymatic assays were performed at 25°C using a spectrophotometer (SPECTROstarNano).

CI (Deamino-NADH:Q reductase) specific activity was measured by a reaction solution comprising Tris–HCl (50 mM, pH 7.2), NaCl (50 mM), FeCN (1 mM), and deamino-NADH (0.2 mM). The decrease in A_{420} was recorded after introducing 10 μg of mitochondrial protein into a 1 ml reaction solution. Specific activity was calculated using an extinction coefficient of 1.03 mM^{-1} cm^{-1} for FeCN at 420 nm (Huang et al., 2015) (n = 3).

CIII (Ubiquinol-cytochrome *c* reductase) specific activity was measured by a reaction solution comprising Tris–HCl (50 mM, pH 7.4), NaN_3 (4 mM), decyl-ubiquinol (0.05 mM), and cytochrome *c* (0.05 mM). The increase of A_{550} was recorded after introducing 10 μg of mitochondrial protein into a 1 ml reaction solution. Specific activity was calculated using an extinction coefficient of 19.6 mM^{-1} cm^{-1} for cytochrome *c* at 550 nm (Luo et al., 2008) (n = 3).

CV (ATP synthase) specific activity was measured by a reaction solution comprising TES-KOH (10 mM, pH 7.2), NaCl (10 mM), $MgSO_4$ (2 mM), bovine serum albumin (0.1% w/v), lactate dehydrogenase (2 units), pyruvate kinase (4 units), KCN (1 mM), NADH (0.2 mM), *n*-propyl-gallate (50 mM), carbonyl cyanide 4-(trifluoromethoxy) phenylhydrazone (5 mM), ATP (1.5 mM), and 50 μg isolated mitochondria subjected to three freeze/thaw cycles

in liquid nitrogen. The increase of A_{340} was recorded after introducing 5 μl of phospho-enol pyruvate (1 mM) into a 1 ml reaction solution. Specific activity was calculated using an extinction coefficient of 6220 $mM^{-1}cm^{-1}$ for NADH at 340 nm (Catterall & Pedersen, 1971) ($n = 3$).

Activity assays were conducted on mitochondria isolated from three independent seedling populations and protein concentrations for each individual sample were quantified using a Bradford assay (Bradford, 1976).

Yeast-2-hybrid interaction assays

Bait constructs (cg-pGBK or n-pGBK) (Stellberger et al., 2010) for B22, along with positive and negative control genes p53 and LAM were transformed into Y187 yeast. Prey constructs (cg-pGAD or n-pGAD) (Stellberger et al., 2010) containing the control gene SV40, CI subunits, including B8, CAL2, CA3, 75 kDa, 23 kDa, PSST, B13, 13 kDa, P1, MNLL (Ivanova et al., 2019), SDAP1, and SDAP2, as well as ISC subunits ISU1, HSCB, HSP23.5, and HSP23.6 (Li et al., 2022) were transformed into AH109 yeast using the PEG/LiAc and DMSO enhanced heat shock method (Gietz & Schiestl, 2007). Selection of transformants was carried out on synthetic defined media (SD): SD−Trp for bait constructs and SD−Leu for prey constructs.

Matings were carried out in 96-well plates using yeast extract peptone dextrose (YPD) liquid medium, following the Matchmaker GAL4 Two-Hybrid System guidelines (Clontech). Mated yeasts were plated on SD−Leu−Trp Double Drop Out (DDO) and SD−Leu−Trp−Ade−His Quadruple Drop Out (QDO) media.

Successfully mated diploid strains were identified after 5 days at 30°C on DDO media, whilst positive protein–protein interaction strains were identified by growth on QDO media. Positive interaction was observed only with B22-cpGBK and SDAP1-npGAD. Variants of B22 were generated by site-directed mutagenesis ($B22^{LAR}$, $B22^{AAA}$, $B22^{A}$) and the mating repeated. The diploid strains were serially diluted in sterile water and plated onto DDO and QDO media.

Bimolecular fluorescence complementation assays

BiFC assays were carried out to confirm the Y2H interactions using transiently transformed protoplasts isolated from 3- to 4-weeks-old Arabidopsis rosette leaves, following the method previously described (Wu et al., 2009). Arabidopsis rosette leaves were sandwiched with tape to remove the lower epidermis layer and then incubated in a freshly prepared enzyme solution (0.5% w/v cellulase, 0.25% w/v pectolyase, 0.1% w/v BSA, 0.4 M mannitol, 20 mM KCl, 20 mM MES pH 5.7, 10 mM $CaCl_2$, sterilised by heating at 55°C for 10 min) for 1 h at 40 rpm under light. Protoplasts were harvested by centrifugation at 70 *g* 4°C for 2 min, washed twice with chilled W5 solution (154 mM NaCl, 125 mM $CaCl_2$, 5 mM KCl, 5 mM glucose, 2 mM MES pH 5.7, sterilised by autoclaving), and incubated on ice for 30 min in the dark. Protoplast concentration was adjusted to approximately 2×10^5 cells ml^{-1} in MMG solution (0.4 M mannitol, 15 mM $MgCl_2$, 5 mM glucose, 4 mM MES pH 5.7, sterilised through a 0.45 μm syringe filter). Transformation was achieved by adding 10 μl of plasmid (1 μg μl^{-1}) and 110 μl of freshly prepared sterile polyethylene glycol (PEG) solution (40% w/v PEG, 0.1 M $CaCl_2$, 0.2 M mannitol) to 300 μl of protoplasts, and incubated for 5 min at room temperature. The transformed mixture was washed twice with 440 μl of W5 solution (centrifuged at 70 *g* for 2 min) and resuspended in 300 μl of W5 solution and incubated overnight in the dark. AOX-RFP was used as a mitochondrial marker to identify cells that had successfully undergone transformation.

Fluorescence was visualised using an Olympus BX61 microscope with excitation/emission wavelengths of 510–535 nm for an enhanced yellow fluorescent protein.

Protein structural prediction

The putative structures for B22, $B22^{LAR}$, $B22^{AAA}$, and $B22^{A}$ and their putative interaction with SDAP1 were predicted using AlphaFold-3, AlphaFold-2 multimer (AF2-MM), and ChAi-1 (Boitreaud et al., 2024; Evans et al., 2022; Jumper et al., 2021). ChimeraX was used to analyse, visualise and annotate the predicted structures, and Blender was used to render the final images (Hess, 2010; Meng et al., 2023).

Statistical analysis

All statistical analyses were carried out by the student's *t*-test with biological replicates as indicated in figure legends (*$P < 0.05$; **$P < 0.01$).

ACCESSION NUMBERS

Sequence data of genes mentioned in this article can be found in The Arabidopsis Information Resource (TAIR) website (Berardini et al., 2015) under the following accession numbers: At1g76060 (ClAF1), At3g12260 (B14), At4g34700 (B22), At5g61220 (ISD11), At5g51960 (FMC1), At3g62810 (MZM1), At3g19508 (SDHAF3), At2g39725 (SDHAF1), At3g18780 (Actin2), At2g42210 (B14.7), At5g13430 (RISP), At5g66760 (SDH1.1), At5g08670 (ATP-β), At3g48680 (CAL2), At1g47260 (CA2), At5g67590 (NDUFS4), At5g11770 (PSST), At3g03070 (13 kDa), At1g67350 (P1), At4g16450 (MNLL), At5g47890 (B8), At1g16700 (23 kDa), At5g52840 (B13), At4g22220 (ISU1), At5g06410 (HSCB), At5g51440 (HSP23.5), At4g25200 (HSP23.6), At1g65290 (SDAP1, mtACP1), At2g44620 (SDAP2, mtACP2), At5g47630 (SDAP3, mtACP3), At5g37510 (75 kDa), and AtMg00160 (Cox2).

ACKNOWLEDGEMENT

Open access publishing facilitated by The University of Western Australia, as part of the Wiley - The University of Western Australia agreement via the Council of Australian University Librarians.

CONFLICT OF INTEREST

The authors declare no conflicts of interest.

DATA AVAILABILITY STATEMENT

The data that supports the findings of this study including predicted protein structures are available in the Supporting Information S1.

SUPPORTING INFORMATION

Additional Supporting Information may be found in the online version of this article.

Figure S1. Characterisation of *b22* T-DNA insertional lines. (a) Gene model highlighting insertions of SAIL_1146 (*b22-1*) and SAIL_1240 (*b22-2*) in B22 (At4g34700). (b) Transcript analysis of *B22* in knockdowns relative to Col-0 determined by quantitative real-time PCR (qRT-PCR). (c) Protein models of B22 with generated

mutants: $B22^{LAR}$, $B22^{A}$, and $B22^{A}$ that was used in generating complementation lines. (d) RNA expression of *b22* in knockdowns and complementation lines relative to Col-0 determined by qRT-PCR. Data represents mean ± SE ($\sigma/\sqrt{?}$); $^{*}P < 0.05$; $^{**}P < 0.01$ (determined by Student's *t*-test, $n = 2$).

Figure S2. Phenotypic analysis of *b22* mutants. (a) Growth stage analysis of *b22* mutants in comparison to Col-0: The development stages are defined as 0.1 = seed imbibition; 0.5 = radical emergence; 0.7 = hypocotyl and cotyledon emergence; 1.0 = fully open cotyledons; 1 + 0.01*n* = '*n*' rosette leaves larger than 1 mm. Scale bar = 2 mm. (b) Relative rosette lengths of *b22* mutants in comparison to Col-0: The longest rosette leaf of each plant was marked after 17 days of sowing and measured every 2–3 days ($n = 18$). Scale bar = 2 cm. (c) Root length analysis of 10-day-old *b22* mutants and Col-0 grown in 0 and 1.5% (w/v) sucrose media ($n = 20$). Scale bar = 1 cm. (d) Hypocotyl elongation of 10-day-old *b22* mutants and Col-0 grown on 1.5% (w/v) sucrose media in the dark ($n > 27$). Scale bar = 0.5 cm. Data represents mean ± S.E ($\sigma/\sqrt{?}$); $^{*}P < 0.05$; $^{**}P < 0.001$ (determined by Student's *t*-test).

Figure S3. Bimolecular fluorescence complementation (BiFC) assays of interaction between known interacting partners, Tim17 and Tim23 (Wang et al., 2012), used as positive control for BiFC assays (Figure 3b). Arabidopsis mesophyll protoplasts were transfected with constructs encoding either the C-terminal or N-terminal half of yellow fluorescent protein (cYFP/nYFP). Scale bar = 20 μm.

Figure S4. Predicted tertiary protein structures of B22 and SDAP1 using AF2-MM (Evans et al., 2022). (a) Predicted structure of B22's interaction with SDAP1 through the LYR domain and the mutated LAR/AAA. Hydrogen bonds (H–N) are represented using dotted lines. (b) Predicted structure of B22's interaction with SDAP1 in the downstream F region and the mutated F → A region.

Figure S5. Predicted tertiary protein structures of B22 and SDAP1 using ChAi-1 (Boitreaud et al., 2024). (a) Predicted structure of B22's interaction with SDAP1 through the LYR domain and the mutated LAR/AAA. Hydrogen bonds (H–N) are represented using dotted lines. (b) Predicted structure of B22's interaction with SDAP1 in the downstream F region and the mutated F → A region.

Figure S6. Predicted average errors (PAE) for SDAP1:B22, SDAP1:$B22^{LAR}$, SDAP1:$B22^{AAA}$, and SDAP1:$B22^{A}$. (a–c) The plots display a heatmap of PAE for structures predicted by AlphaFold-3, AF2-MM, and ChAi-1, respectively. The white dotted lines highlight the interacting region of B22 and SDAP1 that contain pseudo-bonds (>3 Å), as shown in (a).

Figure S7. Relative transcript abundance and phenotypes of *b22-3* mutant. (a) Transcript levels of B22 gene in 7-days-old WT and *b22-3* seedlings. Relative transcript expression was normalised to the nuclear ACT (ACTIN) gene and the B22 line was not plotted as the transcript level was not detectable (ND). Therefore, the cycle threshold (CT) value for this data was taken as 0 for the statistical test. Data represents mean ± SE ($\sigma/\sqrt{?}$); $^{**}P < 0.01$ (determined by Student's *t*-test, $n = 3$). (b) Phenotypes of Col-0 and *b22-3* plants on day 11 after imbibition. (c) Blue Native PolyAcrylamide-Gel Electrophoresis (BN-PAGE) and immunoblotting were conducted on mitochondria isolated from Col-0 and *b22-3*. Mitochondrial proteins were separated in non-denaturing conditions using BN-PAGE and subsequently, transferred onto a PVDF membrane. The proteins were then subjected to Coomassie staining (left), followed by incubation with anti-CA2 antibodies (right).

Table S1. Primers used in this study.

Table S2. Sequences used for multiple sequence alignment (Figure 1b).

REFERENCES

Adam, A.C., Bornhovd, C., Prokisch, H., Neupert, W. & Hell, K. (2006) Nfs1 interacting protein Isd11 has an essential role in Fe/S cluster biogenesis in mitochondria. *The EMBO Journal*, **25**(1), 174–183. Available from: https://doi.org/10.1038/sj.emboj.7600905

Angerer, H. (2015) Eukaryotic LYR proteins interact with mitochondrial protein complexes. *Biology (Basel)*, **4**(1), 133–150. Available from: https://doi.org/10.3390/biology4010133

Angerer, H., Radermacher, M., Mańkowska, M., Steger, M., Zwicker, K., Heide, H. *et al.* (2014) LYR protein subunit NB4M/NDUFA6 of mitochondrial complex I anchors an acyl carrier protein and is essential for catalytic activity. *Proceedings of the National Academy of Sciences of the United States of America*, **111**(14), 5207–5212. Available from: https://doi.org/10.1073/pnas.1322438111

Atkinson, A., Smith, P., Fox, J.L., Cui, T.Z., Khalimonchuk, O. & Winge, D.R. (2011) The LYR protein Mzm1 functions in the insertion of the Rieske Fe/S protein in yeast mitochondria. *Molecular and Cellular Biology*, **31**(19), 3988–3996. Available from: https://doi.org/10.1128/mcb.05673-11

Berardini, T.Z., Reiser, L., Li, D., Mezheritsky, Y., Muller, R., Strait, E. *et al.* (2015) The Arabidopsis information resource: making and mining the "gold standard" annotated reference plant genome. *Genesis (N.Y.)*, **53**(8), 474–485. Available from: https://doi.org/10.1002/dvg.22877

Berrisford, J.M., Baradaran, R. & Sazanov, L.A. (2016) Structure of bacterial respiratory complex I. *Biochimica et Biophysica Acta-Bioenergetics*, **1857**(7), 892–901. Available from: https://doi.org/10.1016/j.bbabio.2016.01.012

Boitreaud, J., Dent, J., McPartlon, M., Meier, J., Reis, V., Rogozhonikov, A. *et al.* (2024) Chai-1: decoding the molecular interactions of life. *bioRxiv*. Available from: https://doi.org/10.1101/2024.10.10.615955

Boniecki, M.T., Freibert, S.A., Mühlenhoff, U., Lill, R. & Cygler, M. (2017) Structure and functional dynamics of the mitochondrial Fe/S cluster synthesis complex. *Nature Communications*, **8**(1), 1287. Available from: https://doi.org/10.1038/s41467-017-01497-1

Boyes, D.C., Zayed, A.M., Ascenzi, R., McCaskill, A.J., Hoffman, N.E., Davis, K.R. *et al.* (2001) Growth stage-based phenotypic analysis of Arabidopsis: a model for high throughput functional genomics in plants. *The Plant Cell*, **13**(7), 1499–1510. Available from: https://doi.org/10.1105/tpc.13.7.1499

Bradford, M.M. (1976) A rapid and sensitive method for the quantitation of microgram quantities of protein utilizing the principle of protein-dye binding. *Analytical Biochemistry*, **72**, 248–254. Available from: https://doi.org/10.1006/abio.1976.9999

Bych, K., Kerscher, S., Netz, D.J., Pierik, A.J., Zwicker, K., Huynen, M.A. *et al.* (2008) The iron-sulphur protein Ind1 is required for effective complex I assembly. *EMBO Journal*, **27**(12), 1736–1746. Available from: https://doi.org/10.1038/emboj.2008.98

Carrie, C., Giraud, E., Duncan, O., Xu, L., Wang, Y., Huang, S. *et al.* (2010) Conserved and novel functions for *Arabidopsis thaliana* MIA40 in assembly of proteins in mitochondria and peroxisomes. *Journal of Biological Chemistry*, **285**(46), 36138–36148. Available from: https://doi.org/10.1074/jbc.M110.121202

Catterall, W.A. & Pedersen, P.L. (1971) Adenosine triphosphatase from rat liver mitochondria. I. Purification, homogeneity, and physical properties. *The Journal of Biological Chemistry*, **246**(16), 4987–4994.

Cory, S.A., Van Vranken, J.G., Brignole, E.J., Patra, S., Winge, D.R., Drennan, C.L. *et al.* (2017) Structure of human Fe–S assembly subcomplex reveals unexpected cysteine desulfurase architecture and acyl-ACP–ISD11 interactions. *Proceedings of the National Academy of Sciences of the United States of America*, **114**(27), E5325–E5334. Available from: https://doi.org/10.1073/pnas.1702849114

Cronan, J.E., Fearnley, I.M. & Walker, J.E. (2005) Mammalian mitochondria contain a soluble acyl carrier protein. *FEBS Letters*, **579**(21), 4892–4896. Available from: https://doi.org/10.1016/j.febslet.2005.07.077

Crooks, G.E., Hon, G., Chandonia, J.-M. & Brenner, S.E. (2004) WebLogo: a sequence logo generator. *Genome Research*, **14**(6), 1188–1190. Available from: https://doi.org/10.1101/gr.849004

Dohnálek, V. & Doležal, P. (2024) Installation of LYRM proteins in early eukaryotes to regulate the metabolic capacity of the emerging mitochondrion. *Open Biology*, **14**(5), 240021. Available from: https://doi.org/10.1098/rsob.240021

Eubel, H., **Braun, H.-P.** & **Millar, A.H.** (2005) Blue-native PAGE in plants: a tool in analysis of protein-protein interactions. *Plant Methods*, **1**(1), 11. Available from: https://doi.org/10.1186/1746-4811-1-11

Evans, R., **O'Neill, M.**, **Pritzel, A.**, **Antropova, N.**, **Senior, A.W.**, **Green, T.** ***et al.*** (2022) *Protein complex prediction with AlphaFold-Multimer*. Cold Spring Harbor: Cold Spring Harbor Laboratory Press.

Floyd, B.J., **Wilkerson, E.M.**, **Veling, M.T.**, **Minogue, C.E.**, **Xia, C.**, **Beebe, E.T.** ***et al.*** (2016) Mitochondrial protein interaction mapping identifies regulators of respiratory chain function. *Molecular Cell*, **63**(4), 621–632. Available from: https://doi.org/10.1016/j.molcel.2016.06.033

Fox, N.G., **Yu, X.**, **Feng, X.**, **Bailey, H.J.**, **Martelli, A.**, **Nabhan, J.F.** ***et al.*** (2019) Structure of the human frataxin-bound iron-sulfur cluster assembly complex provides insight into its activation mechanism. *Nature Communications*, **10**(1), 2210. Available from: https://doi.org/10.1038/s41467-019-09989-y

Fromm, S., **Senkler, J.**, **Eubel, H.**, **Peterhänsel, C.** & **Braun, H.P.** (2016) Life without complex I: proteome analyses of an Arabidopsis mutant lacking the mitochondrial NADH dehydrogenase complex. *Journal of Experimental Botany*, **67**(10), 3079–3093. Available from: https://doi.org/10.1093/jxb/erw165

Fu, X., **Guan, X.**, **Garlock, R.** & **Nikolau, B.J.** (2020) Mitochondrial fatty acid synthase utilizes multiple acyl carrier protein isoforms. *Plant Physiology*, **183**(2), 547–557. Available from: https://doi.org/10.1104/pp.19.01468

Fuchs, P., **Rugen, N.**, **Carrie, C.**, **Elsässer, M.**, **Finkemeier, I.**, **Giese, J.** ***et al.*** (2020) Single organelle function and organization as estimated from Arabidopsis mitochondrial proteomics. *The Plant Journal*, **101**, 420–441. Available from: https://doi.org/10.1111/tpj.14534

Ghifari, A.S., **Saha, S.** & **Murcha, M.W.** (2023) The biogenesis and regulation of the plant oxidative phosphorylation system. *Plant Physiology*, **192**(2), 728–747. Available from: https://doi.org/10.1093/plphys/kiad108

Gietz, R.D. & **Schiestl, R.H.** (2007) High-efficiency yeast transformation using the LiAc/SS carrier DNA/PEG method. *Nature Protocols*, **2**(1), 31–34. Available from: https://doi.org/10.1038/nprot.2007.13

Han, L., **Qin, G.**, **Kang, D.**, **Chen, Z.**, **Gu, H.** & **Qu, L.-J.** (2010) A nuclear-encoded mitochondrial gene AtCIB22 is essential for plant development in Arabidopsis. *Journal of Genetics and Genomics*, **37**(10), 667–683. Available from: https://doi.org/10.1016/S1673-8527(09)60085-0

Herrera, M.a.G., **Pignataro, M.a.F.**, **Noguera, M.n.E.**, **Cruz, K.M.** & **Santos, J.** (2018) Rescuing the rescuer: on the protein complex between the human mitochondrial acyl carrier protein and ISD11. *ACS Chemical Biology*, **13**(6), 1455–1462. Available from: https://doi.org/10.1021/acschembio.8b00184

Hess, R. (2010) *Blender foundations: the essential guide to learning Blender 2.6*. Waltham: Focal Press.

Hofhaus, G., **Weiss, H.** & **Leonard, K.** (1991) Electron microscopic analysis of the peripheral and membrane parts of mitochondrial NADH dehydrogenase (complex I). *Journal of Molecular Biology*, **221**(3), 1027–1043. Available from: https://doi.org/10.1016/0022-2836(91)80190-6

Hua, Y., **Ju, J.**, **Wang, X.**, **Zhang, B.**, **Zhao, W.**, **Zhang, Q.** ***et al.*** (2018) Screening for host proteins interacting with *Escherichia coli* O157:H7 EspF using bimolecular fluorescence complementation. *Future Microbiology*, **13**(1), 37–58. Available from: https://doi.org/10.2217/fmb-2017-0087

Huang, S., **Lee, C.P.** & **Millar, A.H.** (2015) Activity assay for plant mitochondrial enzymes. *Methods in Molecular Biology*, **1305**, 139–149. Available from: https://doi.org/10.1007/978-1-4939-2639-8_10

Itoh, Y., **Khawaja, A.**, **Laptev, I.**, **Cipullo, M.**, **Atanassov, I.**, **Sergiev, P.** ***et al.*** (2022) Mechanism of mitoribosomal small subunit biogenesis and preinitiation. *Nature*, **606**(7914), 603–608. Available from: https://doi.org/10.1038/s41586-022-04795-x

Ivanova, A., **Gill-Hille, M.**, **Huang, S.**, **Branca, R.M.**, **Kmiec, B.**, **Teixeira, P.F.** ***et al.*** (2019) A mitochondrial LyR protein is required for complex I assembly. *Plant Physiology (Bethesda)*, **181**(4), 1632–1650. Available from: https://doi.org/10.1104/pp.19.00822

Jumper, J., **Evans, R.**, **Pritzel, A.**, **Green, T.**, **Figurnov, M.**, **Ronneberger, O.** ***et al.*** (2021) Highly accurate protein structure prediction with AlphaFold. *Nature*, **596**(7873), 583–589. Available from: https://doi.org/10.1038/s41586-021-03819-2

Karimi, M., **Inzé, D.** & **Depicker, A.** (2002) GATEWAY™ vectors for *Agrobacterium*-mediated plant transformation. *Trends in Plant Science*, **7**(5), 193–195. Available from: https://doi.org/10.1016/S1360-1385(02)02251-3

Kastaniotis, A.J., **Autio, K.J.**, **Kerätär, J.M.**, **Monteuuis, G.**, **Mäkelä, A.M.**, **Nair, R.R.** ***et al.*** (2017) Mitochondrial fatty acid synthesis, fatty acids and mitochondrial physiology. *Biochimica et Biophysica Acta, Molecular and Cell Biology of Lipids*, **1862**(1), 39–48. Available from: https://doi.org/10.1016/j.bbalip.2016.08.011

Klepikova, A.V., **Kasianov, A.S.**, **Gerasimov, E.S.**, **Logacheva, M.D.** & **Penin, A.A.** (2016) A high resolution map of the *Arabidopsis thaliana* developmental transcriptome based on RNA-seq profiling. *The Plant Journal*, **88**, 1058–1070. Available from: https://doi.org/10.1111/tpj.13312

Klusch, N., **Dreimann, M.**, **Senkler, J.**, **Rugen, N.**, **Kühlbrandt, W.** & **Braun, H.P.** (2023) Cryo-EM structure of the respiratory I + III(2) supercomplex from *Arabidopsis thaliana* at 2 Å resolution. *Nature Plants*, **9**(1), 142–156. Available from: https://doi.org/10.1038/s41477-022-01308-6

Klusch, N., **Senkler, J.**, **Yildiz, Ö.**, **Kühlbrandt, W.** & **Braun, H.-P.** (2021) A ferredoxin bridge connects the two arms of plant mitochondrial complex I. *The Plant Cell*, **33**(6), 2072–2091. Available from: https://doi.org/10.1093/plcell/koab092

Lefebvre-Legendre, L., **Vaillier, J.**, **Benabdelhak, H.**, **Velours, J.**, **Slonimski, P.P.** & **di Rago, J.P.** (2001) Identification of a nuclear gene (FMC1) required for the assembly/stability of yeast mitochondrial F(1)-ATPase in heat stress conditions. *Journal of Biological Chemistry*, **276**(9), 6789–6796. Available from: https://doi.org/10.1074/jbc.M009557200

Leferink, N.G., **van den Berg, W.A.** & **van Berkel, W.J.** (2008) L-Galactono-gamma-lactone dehydrogenase from *Arabidopsis thaliana*, a flavoprotein involved in vitamin C biosynthesis. *FEBS Journal*, **275**(4), 713–726. Available from: https://doi.org/10.1111/j.1742-4658.2007.06233.x

Letts, J.A., **Fiedorczuk, K.**, **Degliesposti, G.**, **Skehel, M.** & **Sazanov, L.A.** (2019) Structures of respiratory supercomplex I+III(2) reveal functional and conformational crosstalk. *Molecular Cell*, **75**(6), 1131–1146. Available from: https://doi.org/10.1016/j.molcel.2019.07.022

Li, Y., **Belt, K.**, **Alqahtani, S.F.**, **Saha, S.**, **Fenske, R.**, **Van Aken, O.** ***et al.*** (2022) The mitochondrial LYR protein SDHAF1 is required for succinate dehydrogenase activity in Arabidopsis. *Plant Journal*, **110**(2), 499–512. Available from: https://doi.org/10.1111/tpj.15684

Lodish, H.F. (2016) *Molecular cell biology*, 8th edition. New York: W.H. Freeman-Macmillan Learning.

Luo, C., **Long, J.** & **Liu, J.** (2008) An improved spectrophotometric method for a more specific and accurate assay of mitochondrial complex III activity. *Clinica Chimica Acta*, **395**(1), 38–41. Available from: https://doi.org/10.1016/j.cca.2008.04.025

Maio, N., **Singh, A.**, **Uhrigshardt, H.**, **Saxena, N.**, **Tong, W.-H.** & **Rouault, T.A.** (2014) Cochaperone binding to LYR motifs confers specificity of iron sulfur cluster delivery. *Cell Metabolism*, **19**(3), 445–457. Available from: https://doi.org/10.1016/j.cmet.2014.01.015

Masud, A.J., **Kastaniotis, A.J.**, **Rahman, M.T.**, **Autio, K.J.** & **Hiltunen, J.K.** (2019) Mitochondrial acyl carrier protein (ACP) at the interface of metabolic state sensing and mitochondrial function. *Biochimica et Biophysica Acta, Molecular Cell Research*, **1866**(12), 118540. Available from: https://doi.org/10.1016/j.bbamcr.2019.118540

McWilliam, H., **Li, W.**, **Uludag, M.**, **Squizzato, S.**, **Park, Y.M.**, **Buso, N.** ***et al.*** (2013) Analysis tool web services from the EMBL-EBI. *Nucleic Acids Research*, **41**(W1), W597–W600. Available from: https://doi.org/10.1093/nar/gkt376

Meng, E.C., **Goddard, T.D.**, **Pettersen, E.F.**, **Couch, G.S.**, **Pearson, Z.J.**, **Morris, J.H.** ***et al.*** (2023) UCSF ChimeraX: tools for structure building and analysis. *Protein Science*, **32**(11), e4792. Available from: https://doi.org/10.1002/pro.4792

Meyer, E.H., **Heazlewood, J.L.** & **Millar, A.H.** (2007) Mitochondrial acyl carrier proteins in *Arabidopsis thaliana* are predominantly soluble matrix proteins and none can be confirmed as subunits of respiratory complex I. *Plant Molecular Biology*, **64**(3), 319–327. Available from: https://doi.org/10.1007/s11103-007-9156-9

Meyer, E.H., **Tomaz, T.**, **Carroll, A.J.**, **Estavillo, G.**, **Delannoy, E.**, **Tanz, S.K.** ***et al.*** (2009) Remodeled respiration in ndufs4 with low phosphorylation efficiency suppresses Arabidopsis germination and growth and alters control of metabolism at night. *Plant Physiology*, **151**(2), 603–619. Available from: https://doi.org/10.1104/pp.109.141770

Meyer, E.H., **Welchen, E.** & **Carrie, C.** (2019) Assembly of the complexes of the oxidative phosphorylation system in land plant mitochondria. *Annual Review of Plant Biology*, **70**, 23–50. Available from: https://doi.org/10.1146/annurev-arplant-050718-100412

Murcha, M.W. & **Whelan, J.** (2015) Isolation of intact mitochondria from the model plant species *Arabidopsis thaliana* and *Oryza sativa*. *Methods in*

Molecular Biology (Clifton, N.J.), **1305**, 1–12. Available from: https://doi.org/10.1007/978-1-4939-2639-8_1

Niehaus, M., **Straube, H.**, **Künzler, P.**, **Rugen, N.**, **Hegermann, J.**, **Giavalisco, P.** ***et al.*** (2020) Rapid affinity purification of tagged plant mitochondria (Mito-AP) for metabolome and proteome analyses. *Plant Physiology*, **182**, 1194–1210. Available from: https://doi.org/10.1104/pp.19.00736

Nietzel, T., **Mostertz, J.**, **Ruberti, C.**, **Née, G.**, **Fuchs, P.**, **Wagner, S.** ***et al.*** (2020) Redox-mediated kick-start of mitochondrial energy metabolism drives resource-efficient seed germination. *Proceedings of the National Academy of Sciences of the United States of America*, **117**(1), 741–751. Available from: https://doi.org/10.1073/pnas.1910501117

Nowinski, S.M., **Van Vranken, J.G.**, **Dove, K.K.** & **Rutter, J.** (2018) Impact of mitochondrial fatty acid synthesis on mitochondrial biogenesis. *Current Biology*, **28**(20), R1212–R1219. Available from: https://doi.org/10.1016/j.cub.2018.08.022

Perales, M., **Eubel, H.**, **Heinemeyer, J.**, **Colaneri, A.**, **Zabaleta, E.** & **Braun, H.P.** (2005) Disruption of a nuclear gene encoding a mitochondrial gamma carbonic anhydrase reduces complex I and supercomplex I+III2 levels and alters mitochondrial physiology in Arabidopsis. *Journal of Molecular Biology*, **350**(2), 263–277. Available from: https://doi.org/10.1016/j.jmb.2005.04.062

Peters, K., **Nießen, M.**, **Peterhänsel, C.**, **Späth, B.**, **Hölzle, A.**, **Binder, S.** ***et al.*** (2012) Complex I–complex II ratio strongly differs in various organs of *Arabidopsis thaliana*. *Plant Molecular Biology*, **79**(3), 273–284. Available from: https://doi.org/10.1007/s11103-012-9911-4

Schertl, P. & **Braun, H.P.** (2015) Activity measurements of mitochondrial enzymes in native gels. *Methods in Molecular Biology*, **1305**, 131–138. Available from: https://doi.org/10.1007/978-1-4939-2639-8_9

Schertl, P., **Sunderhaus, S.**, **Klodmann, J.**, **Grozeff, G.E.**, **Bartoli, C.G.** & **Braun, H.P.** (2012) L-galactono-1,4-lactone dehydrogenase (GLDH) forms part of three subcomplexes of mitochondrial complex I in *Arabidopsis thaliana*. *Journal of Biological Chemistry*, **287**(18), 14412–14419. Available from: https://doi.org/10.1074/jbc.M111.305144

Schimmeyer, J., **Bock, R.** & **Meyer, E.H.** (2016) L-Galactono-1,4-lactone dehydrogenase is an assembly factor of the membrane arm of mitochondrial complex I in Arabidopsis. *Plant Molecular Biology*, **90**(1–2), 117–126. Available from: https://doi.org/10.1007/s11103-015-0400-4

Schneider, C.A., **Rasband, W.S.** & **Eliceiri, K.W.** (2012) NIH image to ImageJ: 25 years of image analysis. *Nature Methods*, **9**(7), 671–675. Available from: https://doi.org/10.1038/nmeth.2089

Schneider, R., **Massow, M.**, **Lisowsky, T.** & **Weiss, H.** (1995) Different respiratory defective phenotypes of *Neurospora crassa* and *Saccharomyces cerevisiae* after inactivation of the gene encoding the mitochondrial acyl carrier protein. *Current Genetics*, **29**(1), 10–17. Available from: https://doi.org/10.1007/BF00313188

Sheftel, A.D., **Stehling, O.**, **Pierik, A.J.**, **Netz, D.J.**, **Kerscher, S.**, **Elsässer, H.P.** ***et al.*** (2009) Human ind1, an iron-sulfur cluster assembly factor for respiratory complex I. *Molecular and Cellular Biology*, **29**(22), 6059–6073. Available from: https://doi.org/10.1128/mcb.00817-09

Soufari, H., **Parrot, C.**, **Kuhn, L.**, **Waltz, F.** & **Hashem, Y.** (2020) Specific features and assembly of the plant mitochondrial complex I revealed by cryo-EM. *Nature Communications*, **11**(1), 5195. Available from: https://doi.org/10.1038/s41467-020-18814-w

Stellberger, T., **Häuser, R.**, **Baiker, A.**, **Pothineni, V.R.**, **Haas, J.** & **Uetz, P.** (2010) Improving the yeast two-hybrid system with permutated fusions proteins: the varicella zoster virus interactome. *Proteome Science*, **8**(1), 8. Available from: https://doi.org/10.1186/1477-5956-8-8

Sunderhaus, S., **Dudkina, N.V.**, **Jänsch, L.**, **Klodmann, J.**, **Heinemeyer, J.**, **Perales, M.** ***et al.*** (2006) Carbonic anhydrase subunits form a matrix-exposed domain attached to the membrane arm of mitochondrial complex I in plants. *The Journal of Biological Chemistry*, **281**(10), 6482–6488. Available from: https://doi.org/10.1074/jbc.M511542200

Van Vranken, J.G., **Nowinski, S.M.**, **Clowers, K.J.**, **Jeong, M.-Y.**, **Ouyang, Y.**, **Berg, J.A.** ***et al.*** (2018) ACP acylation is an acetyl-CoA-dependent modification required for electron transport chain assembly. *Molecular Cell*, **71**(4), 567–580.e4. Available from: https://doi.org/10.1016/j.molcel.2018.06.039

Wang, G., **Wang, Y.**, **Ni, J.**, **Li, R.**, **Zhu, F.**, **Wang, R.** ***et al.*** (2022) An MCIA-like complex is required for mitochondrial complex I assembly and seed development in maize. *Molecular Plant*, **15**(9), 1470–1487. Available from: https://doi.org/10.1016/j.molp.2022.08.001

Wang, Y., **Carrie, C.**, **Giraud, E.**, **Elhafez, D.**, **Narsai, R.**, **Duncan, O.** ***et al.*** (2012) Dual location of the mitochondrial preprotein transporters B14.7 and Tim23-2 in complex I and the TIM17:23 complex in Arabidopsis links mitochondrial activity and biogenesis. *The Plant Cell*, **24**(6), 2675–2695. Available from: https://doi.org/10.1105/tpc.112.098731

Wirth, C., **Brandt, U.**, **Hunte, C.** & **Zickermann, V.** (2016) Structure and function of mitochondrial complex I. *Biochimica et Biophysica Acta-Bioenergetics*, **1857**(7), 902–914. Available from: https://doi.org/10.1016/j.bbabio.2016.02.013

Wu, F.H., **Shen, S.C.**, **Lee, L.Y.**, **Lee, S.H.**, **Chan, M.T.** & **Lin, C.S.** (2009) Tape-*Arabidopsis* sandwich – a simpler *Arabidopsis* protoplast isolation method. *Plant Methods*, **5**(1), 16. Available from: https://doi.org/10.1186/1746-4811-5-16

Wydro, M.M., **Sharma, P.**, **Foster, J.M.**, **Bych, K.**, **Meyer, E.H.** & **Balk, J.** (2013) The evolutionarily conserved iron-sulfur protein INDH1 is required for complex I assembly and mitochondrial translation in *Arabidopsis* [Corrected title: The evolutionarily conserved iron-sulfur protein INDH is required for complex I assembly and mitochondrial translation in *Arabidopsis*]. *The Plant Cell*, **25**(10), 4014–4027. Available from: https://doi.org/10.1105/tpc.113.117283